Journal of Materials Chemistry A

Accepted Manuscript

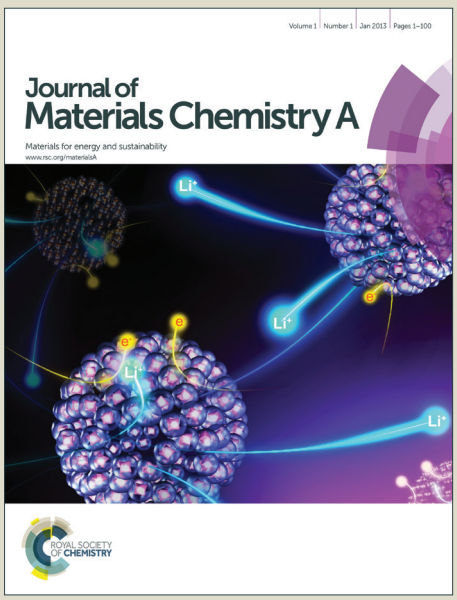

ROYAL SOCIETY OF CHEMISTRY

www.rsc.org/materialsA

ARTICLE

Enhanced Electrochemical Performance of Hierarchical $CoFe_2O_4/MnO_2/C$ Nanotubes as Anode Material for Lithium-Ion Batteries

Cite this: DOI: 10.1039/x0xx00000x

Received 00th 00 2015,
Accepted 00th 00 2015

DOI: 10.1039/x0xx00000x

www.rsc.org/

Junjie Zhou[ab], Ting Yang[a], Minglei Mao[a], Weiji Ren[a], Qiuhong Li[*ab]

Hierarchical $CoFe_2O_4/MnO_2/C$ nanotubes were prepared by electrospinning and a subsequent hydrothermal method. Their electrochemical properties were investigated as anode material for lithium-ion batteries. The $CoFe_2O_4/MnO_2/C$ composite displayed stable cycling performance with a reversible capacity of 713.6 mAh g^{-1} after 250 discharge-charge cycles at a current density of 100 mA g^{-1}, much higher than that of $CoFe_2O_4/C$ nanofibers, which displayed a capacity of 200 mAh g^{-1} after 90 cycles. The improved electrochemical performance could be ascribed to the stable hierarchical structure of the nanocomposite, the existence of carbon, high active surface area, and high theoretical capacity of MnO_2. Given their enhanced electrochemical performance, $CoFe_2O_4/MnO_2/C$ heterostructure composite can be considered as a promising anode for lithium-ion batteries.

1. Introduction

As one of the most important energy-storage devices, lithium-ion batteries (LIBs) have great potential to meet the energy demands of a series of equipments, from portable devices to hybrid electric vehicles because of their high energy density, high voltage, light weight and so on[1-3]. Since the practical applications of LIBs highly rely on the electrodes materials, designing and achieving safe and low-cost electrode materials have turned into a great challenge to both academia and industries[4-6]. Compared with the conventional carbon-based material, transition metal oxides as negative electrodes offer more choices to realize high reversible capacities[7-9]. Recently, cobalt ferrite ($CoFe_2O_4$) has attracted great attention due to its high gravimetric specific capacity (916 mA h g^{-1}), safety, low cost, and environmental friendliness[10-14]. However, like other transition metal oxides, $CoFe_2O_4$ suffers from the problems of poor electrical conductivity and electrode pulverization induced by huge volume changes during the charge-discharge processes, thus leading to poor cycling stability and poor rate capability, which have greatly hampered its practical application[15]. Various strategies have been developed to address these problems[2, 11, 16-18], such as combining $CoFe_2O_4$ with graphene to improve electronic conductivity and structure stability[14, 19], combining $CoFe_2O_4$ with metal oxides to form hierarchical structures to enhance its capacity and strengthen the structure stability [20, 21] and so on.

Hierarchical structures have been considered as promising electrode structure for advanced LIBs because they can not only integrate the merits of individual components, but also take advantage of the nanometer sized secondary building blocks[4, 6, 9, 20-22]. For instance, a high capacity anode for LIBs was fabricated by coating carbon nanotubes (CNTs) with nanosheets MnO_2, combining the advantages of the good electrical conductivity and large surface area of CNTs, and the short path length of MnO_2 nanosheets[23, 24].

Herein, in order to solve the problems of $CoFe_2O_4$ including poor electrical conductivity and poor structural stability, we can add high conductivity carbon to $CoFe_2O_4$. Moreover, constructing heterostructures with other metal oxides serve as a protecting layer to maintain the $CoFe_2O_4$ structural integrity during the bulk redox reaction to achieve the best performance. Manganese dioxide (MnO_2) with high theoretical capacity (1230 mAh g^{-1}), relatively low electrochemical motivation force, and natural abundance[23-26], has been recognized as one of the intensively investigated metal oxides. It was reported that MnO_2 nanoparticles grew onto a conductive polymer or a carbon layer, and the results demonstrated that it could provide a high active surface area and enhance the capacity and stability of the composite[27]. In this work, we grew MnO_2 nanosheets on $CoFe_2O_4/C$ nanofibers to form a heterostructure of $CoFe_2O_4/MnO_2/C$ composite to improve the electrochemical properties.

A facile electrospinning technique combined with a hydrothermal reaction is proposed to synthesize $CoFe_2O_4/MnO_2/C$ nanostructures. The structures incorporated electrochemical features of individual components such as the structural stability of one-dimensional (1D) reticular structure with high theoretical capacity of MnO_2. Thus, on one hand, MnO_2 nanosheets as shell of the composite, effectively separate the as-obtained $CoFe_2O_4$ from the electrolyte, avoiding the possible dissolution of Fe/Co species and other side-effect during charge-discharge process. On the other hand, $CoFe_2O_4$ acts as the core of the composite to effectively restrain the aggregation of newly-formed Mn^0 and accommodate the volume change induced by the reduction of MnO_2[5, 27]. As a result, the prepared material evaluated as anode materials for LIBs exhibited a high initial capacity of 1560 mAh g^{-1} and a stable reversible capacity of 713.6 mAh g^{-1} after 250 cycles at a current density of 100 mA g^{-1}. $CoFe_2O_4/MnO_2/C$ showed enhanced specific capacity, long cycling life and good rate capability. The disclosure of the correlation between the electrochemical properties and the structure/component

of the nanocomposites, would greatly benefit the rational design of the high-performance nanocomposites for lithium ion batteries.

2. Experimental Section

2.1.1 Preparation of $CoFe_2O_4$/C nanofibers.

Firstly, 1 mmol $Co(NO_3)_2 \cdot 6H_2O$ and 2 mmol $Fe(NO_3)_3 \cdot 9H_2O$ were dissolved in a mixture of 2.2 g ethanol and 2.2 g N, N-dimethylformamide and stirred for 1 h at room temperature. Then, 0.37 g polyvinyl pyrrolidone was dissolved in the resulting solution by magnetic stirring for 3 h at room temperature. And then the precursor solutions were pumped through a 10 mL syringe with a stainless steel nozzle (inner diameter is 0.5 mm). The precursor solutions were electrospun by applying a voltage of 20 kV using a high-voltage DC power supply at a distance of 20 cm between the nozzle tip and the collector. Then, the as-obtained nanofibers were dried at 70 °C for 24 h in a vacuum oven, followed by calcination at 450 °C for 2 h with a heating rate of 1 °C min^{-1} under argon.

2.1.2 Fabrication of the $CoFe_2O_4/MnO_2$/C composite.

The prepared 0.2 g $CoFe_2O_4$/C nanofibers and 0.1 g $KMnO_4$ (2:1 W/W) were dissolved in 40 mL deionized water and stirred for 30 min at room temperature. The solution was transferred into a Teflon-lined autoclave and the reaction temperature was maintained at 120 °C for 8 h. After cooling down to room temperature, the resulting black precipitates were washed with distilled water and ethanol several times, and then dried in a vacuum oven at 80 °C overnight.

2.2 Characterization of the $CoFe_2O_4$/C and $CoFe_2O_4/MnO_2$/C material.

The crystal structure of the samples was characterized by X-Ray diffraction (XRD, Cu Kα irradiation) with a SIEMENS D5000 X-ray diffractometer. The morphology and microstructure of the synthesized sample were characterized by scanning electron microscopy (SEM, Hitachi S4800 equipped with an EDS) and a transmission electron microscope (TEM; JEOL-2010) with an accelerating voltage of 200 kV.

2.3 Electrochemical measurements of $CoFe_2O_4$/C and $CoFe_2O_4/MnO_2$/C material.

Electrochemical properties of the $CoFe_2O_4/MnO_2$/C material were evaluated by assembling coin-type cells in an Argon-filled glove box. For preparing the working electrodes, the active material, carbon black and carboxyl methyl cellulose (CMC) were mixed in a weight ratio of 80:10:10, and in distilled water and absolute alcohol mixture, stirred at a constant speed for 12 h to form a homogeneous slurry, which was spread uniformly on a copper foil. The coated copper foil was cut into round pieces with a diameter of 1 cm, and dried at 80 °C in a vacuum overnight. The mass loading of the active material was about 0.8 mg/cm^2. A Celgard 2400 microporous polypropylene membrane was used as a separator. The electrolyte contained a solution of 1 M $LiPF_6$ in ethylene carbonate/dimethyl carbonate/diethyl carbonate (1:1:1, in wt %). These cells were assembled in the glove box (Super 1220/750, Switzerland) filled with highly pure argon gas (O_2 and H_2O levels less than 1 ppm). The cells were aged for 12 h before measurement to ensure percolation of the electrolyte to the electrodes. The cyclic voltammetry and galvanostatic cycling were performed using an Arbin BT2000 system in the voltage of 0.01-3.0 V (vs. Li^+/Li). Nyquist plots were recorded using a CHI660e electrochemical work station at selected voltages ranging from 0.01-3.0 V (vs. Li^+/Li) and frequencies ranging from 0.01 Hz to 1 MHz at room temperature.

3. Results and discussion

The fabrication process of precursor of $CoFe_2O_4$/C nanofibers was presented in step1 of Schematic 1. The growth of $CoFe_2O_4/MnO_2$/C nanocomposite was illustrated in step 2 of Schematic 1. Briefly, the resulting products by step 1 were prepared by calcination at 450 °C for 2 h with a heating rate of 1 °C min^{-1} under argon, and carbon was obtained in $CoFe_2O_4$ nanofibers. And then $CoFe_2O_4$/C nanofibers were dispersed well in a $KMnO_4$ solution at room temperature. Nanocrystalline MnO_2 would be formed on the surface of the $CoFe_2O_4$/C nanofibers due to the slow redox process according to Eq. (1).[28] When the solution was further treated in a hydrothermal reaction, the preformed nanocrystalline MnO_2 acted as nucleation sites for MnO_2 nanosheets to continuously grow due to redox reaction between C and $KMnO_4$ according to Eq. (1) and the decomposition of $KMnO_4$ in water according to Eq. (2). Therefore MnO_2 nanosheets could be uniformly coated on the surfaces of $CoFe_2O_4$/C and $CoFe_2O_4/MnO_2$/C hierarchy nanocomposite was obtained.

$$4MnO_4^- + 3C + H_2O \rightarrow 4MnO_2 + CO_3^{2-} + 2HCO_3^- \quad (1)$$

$$4MnO_4^- + 2H_2O \rightarrow 4MnO_2 + 4OH^- + 3O_2 \quad (2)$$

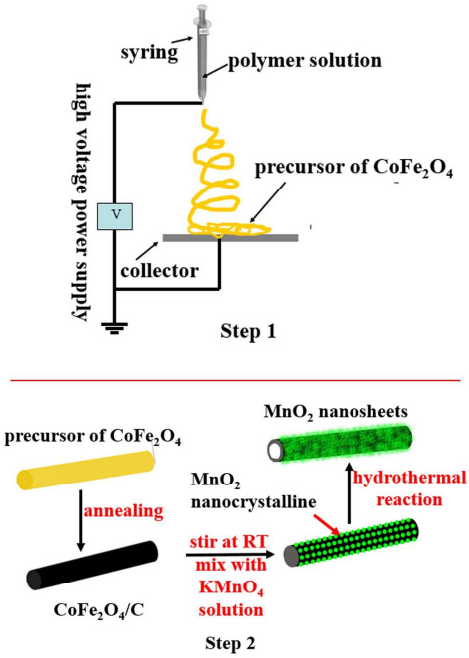

Schematic 1 Illustration of synthesis process of $CoFe_2O_4/MnO_2$ /C nanotubes.

The SEM image of the $CoFe_2O_4$/C nanofibers was shown in Fig. 1a. The $CoFe_2O_4$/C fibers exhibited smooth surface morphology with diameters ranging from 50 to 90 nm. Moreover, from Fig. S1a (in the Supporting Information) we could see the $CoFe_2O_4$/C nanofibers were in solid structure. Fig. 1b-d showed SEM images of the $CoFe_2O_4/MnO_2$/C composite. Obviously, after coating MnO_2 nanosheets, the composite not only became thick with diameters larger than 100 nm, but also became rough and brushy. It was seen

from Fig. 1c-d that the MnO_2 nanosheets uniformly coated on $CoFe_2O_4$/C nanotubes to form a core-shell structure with plenty of room which could alleviate volume change during lithium-ion intercalation-deintercalation process. As shown in Fig. 1d, the $CoFe_2O_4/MnO_2$/C composite was hollow, and the diameter of the holes was about 40 nm, which could not only effectively shorten lithium-ion and electron transport path along the 1D geometry hollow nanotubes, but also alleviate volume change of $CoFe_2O_4$ during charge-discharge process. Moreover, Fig. S1b (in the Supporting Information) further showed that $CoFe_2O_4/MnO_2$/C composite was in hollow structure. By comparing Fig. S1a with Fig. S1b, we could know solid structure of $CoFe_2O_4$/C nanofibers transformed into hollow structure of $CoFe_2O_4/MnO_2$/C composite via the hydrothermal reaction, which could be induced by the consumption of partial carbon of $CoFe_2O_4$/C nanofibers due to the redox reaction between C and $KMnO_4$ according to Eq. (1) during the hydrothermal reaction. Moreover, by comparing Fig. 1a with Fig. S1b, $CoFe_2O_4/MnO_2$/C nanotubes were in decreased length after the hydrothermal reaction. The reason that $CoFe_2O_4$/C nanofibers appeared fractured could be related with the reaction of $KMnO_4$ with carbon in $CoFe_2O_4$/C fibers during MnO_2 coating process. As shown in Fig. 1b-c, after coating MnO_2 nanosheets, $CoFe_2O_4/MnO_2$/C nanotube was connected to each other to form a reticular structure, thus leading to good structure stability of $CoFe_2O_4/MnO_2$/C electrodes during charge-discharge process.

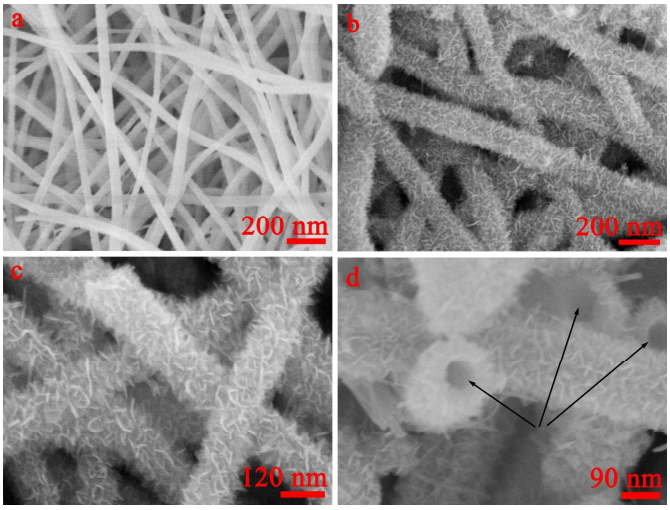

Figure 1 SEM images of (a) $CoFe_2O_4$/C nanofibers; (b-d) $CoFe_2O_4/MnO_2$/C composite at different magnifications.

The detailed structure of the products was also examined by TEM. Fig. 2a displayed TEM image of $CoFe_2O_4$/C fibers. Fig. 2b showed typical TEM images of the $CoFe_2O_4/MnO_2$/C composite in which ultrathin MnO_2 nanosheets were uniformly distributed on the surface of the $CoFe_2O_4$/C. A close examination of the exposed profile revealed that the thickness of the outer MnO_2 layer was about 30 nm. The high-resolution TEM (HRTEM) image of $CoFe_2O_4/MnO_2$/C hybrid structure shown in Fig. 2d revealed two interplanar spacings of 0.25 nm and 0.48 nm, corresponding to the (311) and (111) planes of $CoFe_2O_4$[14], respectively. An interplanar spacing of 0.46 nm corresponded to the (111) plane of MnO_2[26], which was in agreement with the XRD result (Fig. 3).

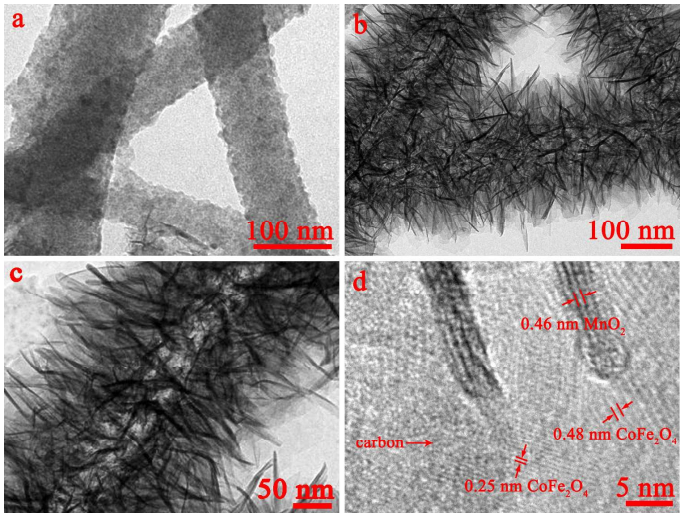

Figure 2 (a) TEM image of $CoFe_2O_4$/C nanofibers; (b-c) TEM images of $CoFe_2O_4/MnO_2$/C composite; (d) HRTEM image of $CoFe_2O_4/MnO_2$/C composite.

Fig. 3 showed the XRD pattern of the as-prepared $CoFe_2O_4/MnO_2$/C nanotubes. The three diffraction peaks appear at 30.28°, 35.54° and 62.58°, which can be respectively attributed to (220), (311) and (440) reflections of the spinel $CoFe_2O_4$ (JCPDS 22-1086). The diffraction peaks appear at 19.22°, 37.14°, 45.02° and 67.21° are attributed to (111), (311), (400) and (531) reflections of MnO_2 (JCPDS 42-1169). A broad band at about 25.6° can be indexed to the carbon phase[13]. The XRD pattern revealed that the resulting sample consisted of $CoFe_2O_4$, MnO_2 and amorphous carbon. We also carried out energy dispersive spectroscopic (EDS) analysis of the composite. The EDS spectrum was shown in Figure S2 in the Supporting Information. The result indicated the existence of manganese, iron, cobalt, and carbon in the composite. Thermogravimetric analysis (TGA) was conducted to estimate the carbon weight in the composite, which was about 31 wt% as indicated in Figure S3 in the Supporting Information.

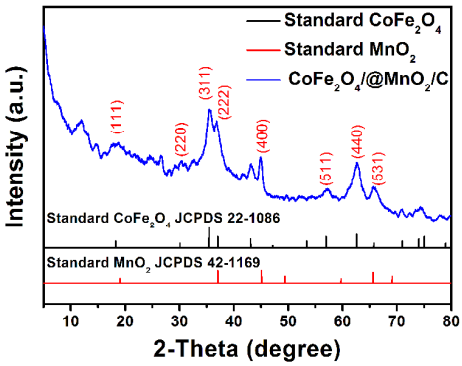

Figure 3 XRD pattern of the $CoFe_2O_4/MnO_2$/C composite (blue), standard $CoFe_2O_4$ (black) and standard MnO_2 (red).

Fig. 4 showed the cyclic voltammograms of the $CoFe_2O_4/MnO_2$/C electrode between 0.01 and 3.00 V (vs. Li/Li^+) at a scan rate of 0.1 mV s^{-1}. In the first cycle, a cathodic peak at about 0.2 V could be ascribed to the reduction of MnO_2 to metallic manganese as well as the formation of solid electrolyte interface (SEI), and the other cathodic peak at around 0.59 V could be attributed to the reduction of Fe^{3+} and Co^{2+} to their metallic states and the formation of Li_2O and SEI. In the anodic process, an anodic peak at about 1.2 V

corresponded to the oxidation of metallic manganese[26]. And a broad peak at around 1.8 V could be ascribed to the multi-oxidation steps of metallic Co and Fe to Co^{2+} and Fe^{3+}, respectively[29]. Compared with the first cycle, due to the structure reconstruction induced by the formation of Li_2O and metals, the cathodic peaks of the subsequent cycles shifted to higher potentials, which further confirmed multi-step electrochemical reactions[30]. An obvious decrease of the areas enclosed by CV curves from the first to the second cycle indicated an irreversible capacity loss in the initial lithiation/delithiation process, usually attributing to the occurrence of irreversible reactions associated with formation of an SEI layer. The results, to a certain extent, sustained the electrochemical reactions for the anode material as follows:

$$CoFe_2O_4 + 8Li^+ + 8e^- \rightarrow Co + 2Fe + 4Li_2O \quad (3)$$

$$Co + Li_2O \leftrightarrow CoO + 2Li^+ + 2e^- \quad (4)$$

$$2Fe + 3Li_2O \leftrightarrow Fe_2O_3 + 6Li^+ + 6e^- \quad (5)$$

$$MnO_2 + 4Li^+ + 4e^- \leftrightarrow 2Li_2O + Mn \quad (6)$$

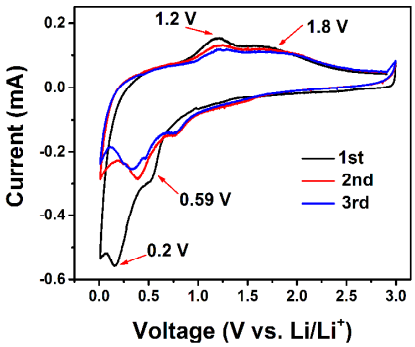

Figure 4 Cyclic voltammetry (CV) of $CoFe_2O_4/MnO_2/C$ composite at a scan rate of 0.1 mV s^{-1}.

The charge-discharge curves for the prepared $CoFe_2O_4/C$ and $CoFe_2O_4/MnO_2/C$ anodes with a current density of 100 mA g^{-1} were shown in Fig. 5a-b. The initial charge capacities were 970.9 mAh g^{-1} for $CoFe_2O_4/C$, and 1583.8 mAh g^{-1} for $CoFe_2O_4/MnO_2/C$ electrode, respectively. The increased capacity for $CoFe_2O_4/MnO_2/C$ nanocomposite was not only from mechanical amalgamation, but an inter-enhancement effect of these two compositions [21]. The large capacity loss in the first cycle for these electrodes was caused by the formation of SEI on the electrode surface due to the electrolyte decomposition[31-33]. Fig. 5b clearly showed a voltage plateau at 0.59 V in the first discharge, reflecting the conversion reaction of Fe^{3+} and Co^{2+} to their metallic states [34], which was in agreement with the result in Fig. 4 of cyclic voltammetry (CV) for $CoFe_2O_4/MnO_2/C$ composite.

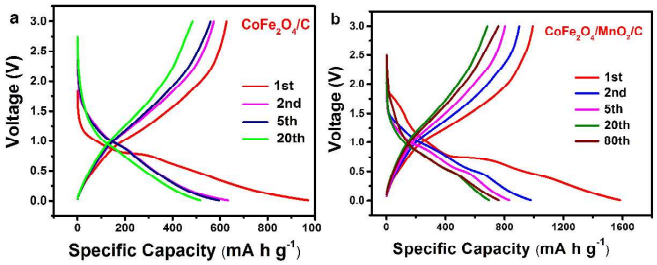

Figure 5 Charge-discharge curves of (a) $CoFe_2O_4/C$, and (b) $CoFe_2O_4/MnO_2/C$ at a current density of 100 mA g^{-1}.

Stable cyclic performance of electrode material is important for practical application of LIBs. The cycling stabilities of the $CoFe_2O_4/MnO_2/C$ composite and $CoFe_2O_4/C$ nanofibers were investigated at a current density of 100 mA g^{-1} between 0.01 and 3.0 V (Fig. 6a). The discharge capacity of the $CoFe_2O_4/MnO_2/C$ electrode remained 713.6 mAh g^{-1} after 250 cycles, and the coulumbic efficiency was around 99%, indicating a stable cyclability. In contrast, the $CoFe_2O_4/C$ nanofibers only delivered a much lower capacity of 200 mAh g^{-1} after 90 discharge-charge cycles. Moreover, the capacity of $CoFe_2O_4/MnO_2/C$ increased slightly with cycling, which was also observed in many metal oxide anode materials.[35-37] The reasons for the increase of capacity during cycling could be ascribed to the reversible growth of a polymer gel-like film caused by kinetically activated electrolyte degradation and the activation of the active materials. [38-42] The high electrochemical performance of the core-shell nanomaterials was mainly related with the following factors: (1) the hollow structure could not only facilitate lithium-ion access, but also accommodate large volumetric expansion to slow the rate of electrode pulverization; (2) MnO_2 nanosheets and high conductivity of carbon buffer layers served as protecting layers to maintain the structural integrity during the bulk redox reaction; after coating MnO_2 nanosheets, $CoFe_2O_4/MnO_2/C$ nanotubes were connected to each other to form a reticular structure, thus leading to good structure stability of $CoFe_2O_4/MnO_2/C$ electrodes; (3) MnO_2 nanosheets as the shells of the composite, effectively separated the as-obtained $CoFe_2O_4$ from the electrolyte, avoiding the possible dissolution of Fe/Co species and other side-effect during charge-discharge process. Meanwhile, $CoFe_2O_4$ acted as a core to restrain the aggregation of newly-formed Mn^0 and accommodate the volume change induced by the reduction of MnO_2[5, 27]. $CoFe_2O_4/MnO_2/C$ nanotubes showed enhanced cycling properties, better than a series of reported $CoFe_2O_4$ or MnO_2 composites. As shown in Tabel S1, long stable cycling and high capacity were featured as compared with some reported $CoFe_2O_4$ and MnO_2 materials or their composites.

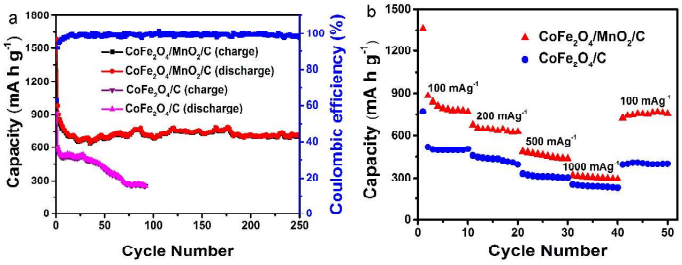

Figure 6 (a) Cycling performance of $CoFe_2O_4/C$ and $CoFe_2O_4/MnO_2/C$ heterostructure at a current density of 100 mA g^{-1}. (b) Rate performance of $CoFe_2O_4/MnO_2/C$ composite and $CoFe_2O_4/C$ anodes.

To examine the rate performance of the $CoFe_2O_4/MnO_2/C$ electrode, the discharge capacities of $CoFe_2O_4/MnO_2/C$ were measured at different discharge current densities. Fig. 6b showed the rate performance of $CoFe_2O_4/MnO_2/C$ and $CoFe_2O_4/C$ electrodes. For $CoFe_2O_4/MnO_2/C$, the average discharge capacities of 799.8, 648.8, 470.4, and 310.6 mAh g^{-1} were observed at the current densities of 100, 200, 500, and 1000 mA g^{-1}, respectively. For comparison, $CoFe_2O_4/C$ delivered capacities of 497.9, 423.5, 310.8, and 237.8 mAh g^{-1}, when the current densities were 100, 200, 500 and 1 000 mA g^{-1}, respectively. When the current density was returned to 100 mA g^{-1}, the discharge capacity of the $CoFe_2O_4/MnO_2/C$ electrode could recover to 762.9 mAh g^{-1}. However, the $CoFe_2O_4/C$ electrode only displayed a capacity of 397

mAh g^{-1}. The enhanced rate performance of the $CoFe_2O_4/MnO_2/C$ electrode was related with the following properties: firstly, the hollow structure allowed the electrolyte easily diffusing into the interior of the composite and reduced the resistance of the transported lithium-ion; secondly, the high surface area increased the contact between the electrode and electrolyte and provided a large number of potential active sites for Li^+ transfer reaction; thirdly, the existence of carbon layer improved the conductivity of the electrode. The high capacity achieved at a high cycling rate implies that this type of electrode can be a promising candidate for high power application.

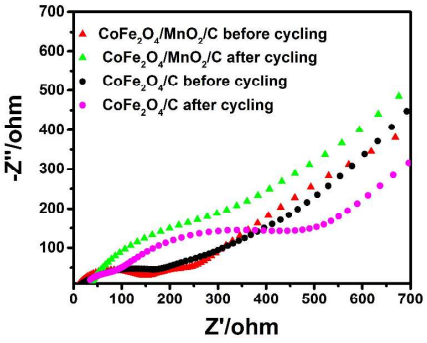

Figure 7 Impedance spectra of $CoFe_2O_4/C$ and $CoFe_2O_4/MnO_2/C$ electrodes.

Electrochemical impedance spectroscopy (EIS) provide detailed information on charge transfer, surface film, bulk resistance and capacitance of the electrodes.[43] EIS were carried out on $CoFe_2O_4/MnO_2/C$ at selected frequencies ranging from 0.01 Hz to 1 MHz at room temperature. All impedance spectrum exhibited a single semicircle at high frequency region, which was related with the charge transfer resistance (R_{ct}), and a sloping line at low frequency region, representing the Warburg impedance (Z_w) induced by lithium-ion diffusion in the electrodes [44]. Fig. 7 showed the electrochemical impedance of $CoFe_2O_4/MnO_2/C$ and $CoFe_2O_4/C$ before cycling and after 200 cycles. Before cycling, R_{ct} of $CoFe_2O_4/MnO_2/C$ and $CoFe_2O_4/C$ displayed little difference. After 200 cycles, it was obvious that R_{ct} of $CoFe_2O_4/MnO_2/C$ was lower than that of $CoFe_2O_4/C$. As expected, the hierarchical $CoFe_2O_4/MnO_2/C$ nanotube electrode possessed a rapid charge transfer reaction during lithium insertion and extraction. The result indicated that $CoFe_2O_4/MnO_2/C$ nanocomposite electrode possessed enhanced electrochemical performance.

4. Conclusions

In summary, an electrospinning and sequent hydrothermal method was developed to synthesize core-shell $CoFe_2O_4/MnO_2/C$ nanotubes. The hollow core-shell structure provided sufficient electrode-electrolyte interface and alleviated the large strain caused by the conversion reaction of electrode, and was also beneficial to the lithium-ion and electron transportation. As a result, the $CoFe_2O_4/MnO_2/C$ heterostructure anode showed a high initial capacity of 1580.6 mAh g^{-1} and a reversible capacity of 713.6 mAh g^{-1} after 250 cycles at 100 mA g^{-1}, a long cycling life and good rate performance. The highly improved electrochemical performance was ascribed to stable hierarchical structure of the nanocomposite, the existence of the carbon layer, high active surface area and high theoretical capacity of MnO_2. MnO_2 sheet was proposed to serve as a protecting layer to maintain the $CoFe_2O_4$ structural integrity during the bulk redox reaction. The $CoFe_2O_4/MnO_2/C$ heterostructure are promising anode materials for LIBS.

Acknowledgments

This work was partly supported from the Specialized Research Fund for the Doctoral Program of Higher Education of China (20120161110016), and the National Natural Science Foundation of China (Grant No. 61376073).

Notes and references

[a] Key laboratory for Micro-/Nano-Optoelectronic Devices of Ministry of Education, School of Physics and Electronics, Hunan University, Changsha 410082, China. E-mail address: liqiuhong@xmu.edu.cn. Tel.: 86-592-2187198.
[b] Pen-Tung Sah Institute of Micro-Nano Science and Technology of Xiamen University, Xiamen, 361005, China.

1. J. G. Kim, S. H. Lee, Y. Kim and W. B. Kim, *ACS Applied Materials & Interfaces*, 2013, 5, 11321-11328.
2. N. Wang, H. Xu, L. Chen, X. Gu, J. Yang and Y. Qian, *Journal of Power Sources*, 2014, 247, 163-169.
3. Z. Xing, Z. Ju, J. Yang, H. Xu and Y. Qian, *Nano Res.*, 2012, 5, 477-485.
4. R. Zhang, Y. He, A. Li and L. Xu, *Nanoscale*, 2014, 6, 14221-14226.
5. X. Gu, L. Chen, Z. Ju, H. Xu, J. Yang and Y. Qian, *Advanced Functional Materials*, 2013, 23, 4049-4056.
6. Q. Q. Xiong, J. P. Tu, X. H. Xia, X. Y. Zhao, C. D. Gu and X. L. Wang, *Nanoscale*, 2013, 5, 7906-7912.
7. G. Wang, R. Chen, Y. Zhou, H. Wang, J. Bai, *Journal of Nanoparticle Research*, 2014, 16, 2300.
8. J. Liu, J. Jiang, M. Bosman and H. J. Fan, *Journal of Materials Chemistry*, 2012, 22, 2419-2426.
9. A. K. Rai, J. Gim, T. V. Thi, D. Ahn, S. J. Cho and J. Kim, *the Journal of Physical Chemistry C*, 2014, 118, 11234-11243.
10. Y. N. NuLi and Q. Z. Qin, *Journal of Power Sources*, 2005, 142, 292-297.
11. Y. Q. Chu, Z. W. Fu and Q. Z. Qin, *Electrochimica Acta*, 2004, 49, 4915-4921.
12. Y. Wang, D. Su, A. Ung, J. Ahn and G. Wang, *Nanotechnology*, 2012, 23, 055402.
13. L. Wu, Q. Xiao, Z. Li, G. Lei, P. Zhang and L. Wang, *Solid State Ionics*, 2012, 215, 24-28.
14. H. Xia, D. Zhu, Y. Fu and X. Wang, *Electrochimica Acta*, 2012, 83, 166-174.
15. Z. H. Li, T. P. Zhao, X. Y. Zhan, D. S. Gao, Q. Z. Xiao and G. T. Lei, *Electrochimica Acta*, 2010, 55, 4594-4598.
16. Z. Zhang, Y. Wang, M. Zhang, Q. Tan, X. Lv, Z. Zhong and F. Su, *Journal of Materials Chemistry A*, 2013, 1, 7444-7450.
17. H. Xia, D. Zhu, Y. Fu, Xin Wang, *Electrochimica Acta*, 2012, 83, 166-174.
18. S. Li, A. Li, R. Zhang, Y. He, Y. Zhai, L. Xu, *Nano Research*, 2014, 7, 1116-1127.
19. Y. Yao, Z. Yang, D. Zhang, W. Peng, H. Sun and S. Wang, *Industrial & Engineering Chemistry Research*, 2012, 51, 6044-6051.
20. G. Huang, F. Zhang, X. Du, J. Wang, D. Yin and L. Wang, *Chemistry – A European Journal*, 2014, 20, 11214-11219.
21. X. Li, Y. Chen, H. Yao, X. Zhou, J. Yang, H. Huang, Y.-W. Mai and L. Zhou, *RSC Advances*, 2014, 4, 39906-39911.
22. B. Wang, X. He, H. Li, Q. Liu, J. Wang, L. Yu, H. Yan, Z. Li and P. Wang, *Journal of Materials Chemistry A*, 2014, 2, 12968-12973.
23. J. Zhao, Z. Tao, J. Liang and J. Chen, *Crystal Growth & Design*, 2008, 8, 2799-2805.
24. H. Lai, J. Li, Z. Chen and Z. Huang, *ACS Applied Materials & Interfaces*, 2012, 4, 2325-2328.
25. L. Li, A. R. O. Raji and J. M. Tour, *Advanced Materials*, 2013, 25, 6298-6302.
26. H. Xia, M. Lai and L. Lu, *Journal of Materials Chemistry*, 2010, 20, 6896-6902.

27. J. Liu, J. Jiang, C. Cheng, H. Li, J. Zhang, H. Gong and H. J. Fan, *Advanced Materials*, 2011, 23, 2076-2081.
28. C. X. Guo, M. Wang, T. Chen, X. W. Lou and C. M. Li, *Advanced Energy Materials*, 2011, 1, 736-741.
29. X. Yao, J. Kong, X. Tang, D. Zhou, C. Zhao, R. Zhou and X. Lu, *RSC Advances*, 2014, 4, 27488-27492.
30. Y. Wang, J. Park, B. Sun, H. Ahn and G. Wang, *Chemistry-An Asian Journal*, 2012, 7, 1940.
31. B. Zhang, Y. Liu, Z. Huang, S. Oh, Y. Yu, Y. W. Mai and J. K. Kim, *Journal of Materials Chemistry*, 2012, 22, 12133-12140.
32. X. Li, Y. Chen, L. Zhou, Y.-W. Mai and H. Huang, *Journal of Materials Chemistry A*, 2014, 2, 3875-3880.
33. L. Wang, Y. Li, Z. Han, L. Chen, B. Qian, X. Jiang, J. Pinto and G. Yang, *Journal of Materials Chemistry A*, 2013, 1, 8385-8397.
34. W. Xiao, J. S. Chen, Q. Lu and X. W. Lou, *the Journal of Physical Chemistry C*, 2010, 114, 12048-12051.
35. P. L. Taberna, S. Mitra, P. Poizot, P. Simon and J. M. Tarascon, *Nature Materials*, 2006, 5, 567-573.
36. Y. Fu, X. Li, X. Sun, X. Wang, D. Liu and D. He, *Journal of Materials Chemistry*, 2012, 22, 17429-17431.
37. Y. Xia, W. Zhang, Z. Xiao, H. Huang, H. Zeng, X. Chen, F. Chen, Y. Gan and X. Tao, *Journal of Materials Chemistry*, 2012, 22, 9209-9215.
38. S. Grugeon, S. Laruelle, L. Dupont and J. M. Tarascon, *Solid State Sciences*, 2003, 5, 895-904.
39. S. Laruelle, S. Grugeon, P. Poizot, M. Dollé, L. Dupont and J.-M. Tarascon, *Journal of the Electrochemical Society*, 2002, 149, A627-A634.
40. Y. Yu, C. H. Chen, J. L. Shui and S. Xie, *Angewandte Chemie International Edition*, 2005, 44, 7085-7089.
41. L. Yu, Z. Wang, L. Zhang, H. B. Wu and X. W. Lou, *Journal of Materials Chemistry A*, 2013, 1, 122-127.
42. Y. Lu, K. Qiu, D. Zhang, J. Lin, J. Xu, X. Liu, C. Tang, J.-K. Kim and Y. Luo, *RSC Advances*, 2014, 4, 46814-46822.
43. B. Das, M. V. Reddy, C. Krishnamoorthi, S. Tripathy, R. Mahendiran, G. V. S. Rao and B. V. R. Chowdari, *Electrochimica Acta*, 2009, 54, 3360-3373.
44. S. Hu, F. Yin, E. Uchaker, W. Chen, M. Zhang, J. Zhou, Y. Qi and G. Cao, *the Journal of Physical Chemistry C*, 2014, 118, 24890-24897.

We report a facile approach to prepare MnO_2 nanosheets coated $CoFe_2O_4$ nanofibers containing carbon for lithium ion batteries by electrospinning and subsequent hydrothermal process. The $CoFe_2O_4/MnO_2/C$ nanotubes exhibit a reversible capacity of 713.6 mAh g^{-1} at 100 mA g^{-1} after 250 cycles with highly stable capacity retention.